1 **Alteration of the size distributions and mixing states of black**

2 **carbon through transport in the boundary layer in East Asia**

4 Takuma Miyakawa[1 2], Naga Oshima[3], Fumikazu Taketani[1 2], Yuichi Komazaki[1], Ayako

5 Yoshino[4], Akinori Takami[4], Yutaka Kondo[5], and Yugo Kanaya[1 2]

6 [1]Department of Environmental Geochemical Cycle Research, Japan Agency for Marine-

7 Earth Science and Technology, 3173-25 Showa-machi, Kanazawa-ku, Yokohama,

8 Kanagawa, 236-0001, Japan.

9 [2]Institute for Arctic Climate Environment Research, Japan Agency for Marine-Earth

10 Science and Technology, 3173-25 Showa-machi, Kanazawa-ku, Yokohama, Kanagawa,

11 236-0001, Japan.

12 [3]Meteorological Research Institute, 1-1 Nagamine, Tsukuba, Ibaraki, 305-0052, Japan

13 [4]Center for Regional Environmental Research, National Institute for Environmental

14 Studies, 16-2 Onogawa, Tsukuba, Ibaraki, 305-8506, Japan

15 [5]National Institute for Polar Research, 10-3 Midori-cho, Tachikawa, Tokyo, 190-8518,

16 Japan

17 *Correspondence to*: Takuma Miyakawa (miyakawat@jamstec.go.jp)

19 **Abstract.** Ground-based measurements of black carbon (BC) were performed near an

20 industrial source region in the early summer of 2014 and at a remote island in Japan in

21 the spring of 2015. Here, we report the temporal variations in the transport, size

22 distributions, and mixing states of the BC-containing particles. These particles were

23 characterized using a continuous soot monitoring system, a single particle soot

24   photometer, and an aerosol chemical speciation monitor.   The effects of aging on the

25   growth of BC-containing particles were examined by comparing the ground-based

26   observations between the near-source and remote island sites.   Secondary formation of

27   sulfate aerosols through gas- and cloud-phase reactions strongly affected the increases in

28   BC coating (i.e., enhancement of cloud condensation nuclei activity) with air mass aging

29   from the source to the outflow regions.   The effects of wet removal on BC microphysics

30   were elucidated by classifying the continental outflow air masses depending on the

31   enhancement ratios of BC to CO (ΔBC/ΔCO) ratios, which was used as an indicator of

32   the transport efficiency of BC.   It was found that ΔBC/ΔCO ratios were controlled

33   mainly by the rainout process during transport in the planetary boundary layer (PBL) on

34   the timescale of 1-2 days.   The meteorological conditions and backward trajectory

35   analyses suggested that air masses strongly affected by rainout originated mainly from a

36   region in South China (20º-35ºN) in the spring of 2015.   Selective removal of large and

37   thickly-coated BC-containing particles was detected in the air masses that were

38   substantially affected by the rainout in the PBL, as predicted by Köhler theory.   The size

39   and water-solubility of BC-containing particles in the PBL can be altered by the rainout

40   process as well as the condensation of non-BC materials.

42   **1. Introduction**

43   Black carbon (BC)-containing particles in atmosphere can significantly affect the

44   radiative budget of the Earth through two effects; direct (light absorption and scattering)

45   and indirect (aerosol-cloud interactions) effects (Bond et al., 2013; references therein).

46   The difficulty in the estimation of these effects in the atmosphere results from both the

47   short lifetime relative to other greenhouse gases and the variable physicochemical

48   properties of BC-containing particles.   The BC itself is water-insoluble immediately

49   after emission, but it subsequently exhibits on hygroscopicity (McMeeking et al., 2011)

50   and cloud condensation nuclei (CCN) activity (Kuwata et al., 2007) through atmospheric

51   transport and aging.   Only small amounts of water-soluble materials on BC particles are

52   needed to cause their activation to form cloud droplets under moderate supersaturation

53   conditions (Kuwata et al., 2007; 2009).   It is considered that BC-containing particles are

54   removed from the atmosphere mainly by wet deposition (Seinfeld and Pandis, 2006).

55   The horizontal and vertical distributions of aerosols can be substantially altered by their

56   atmospheric lifetimes (e.g., Lawrence et al., 2007).   Moreover, their studies suggested

57   that the removal processes of BC such as dry deposition, below-cloud (i.e., washout), and

58   in-cloud (i.e., rainout) can greatly change the atmospheric lifetimes.   The in-cloud

59   processes include nucleation scavenging and scavenging by the preexisting cloud droplets.

60   Precipitation followed by in-cloud processes leads to the irreversible removal of BC-

61   containing particles.   Samset et al. (2014), using multiple global model data sets

62   constrained by aircraft observations, suggested that the atmospheric lifetime of BC

63   largely affects its distribution, especially in the northern hemisphere, and this results in

64   significant variations in global direct radiative forcing values.   The removal of BC has

65   been considered as an important issue for the geochemical carbon cycle as well as for

66   climate science.   The BC-containing particles deposited onto the ocean surface can

67   affect ocean surface particles, dissolved organic carbon (DOC), and microbial processes,

68   by absorbing DOC, stimulating particle aggregation, and changing the size distribution

69   of suspended particles (Mari et al., 2014).

70   Previous modeling studies have dealt with BC aging processes (condensational growth

71   and coagulation) in box and regional-scale models, and parameterized timescales for the

72   conversion of BC-containing particles from water-insoluble to -soluble in global models

73   (Oshima et al., 2009; Liu et al., 2011; Oshima and Koike, 2013).   However, quantitative

74   knowledge of the variability of microphysical parameters of BC-containing particles and

75   the timescale of their aging processes is still limited, and thus more investigation are

76   needed for near-source and remote regions (Samset et al., 2014).   Moteki et al. (2012)

77   reported the first observational evidence of the size-dependent activation of BC during

78   the cloud droplets formation, in air masses uplifting from the planetary boundary layer

79   (PBL) to the free troposphere (FT) in East Asia in the spring of 2009, as the part of the

80   Aerosol Radiative Forcing in East Asia (A-FORCE) aircraft campaigns (Oshima et al.,

81   2012).   A similar altitude dependence of the BC size distribution and similarity in the

82   BC mixing state were observed in other aircraft measurements conducted in East Asia in

83   winter (Kondo et al., 2016).   Selective removal of larger BC-containing particles though

84   the cloud process, which is predicted by Köhler theory, was qualitatively observed in the

85   atmosphere.   This observational evidence indicates that the size distributions and mixing

86   states of BC-containing particles control the global- and regional-scale spatial

87   distributions of BC through their upward transport from the PBL to the FT associated

88   with rainout processes.   Despite the importance of the size distributions and mixing

89   states of BC-containing particles in the PBL, the measurements of their microphysical

90   properties are still limited around the source regions in East Asia.

91   Kanaya et al. (2016) have conducted long-term measurements of BC for 6 years (2009-

92   2015) at Fukue Island, and they synthetically reported the emission and removal of BC

93   in East Asia using these data sets.   It was found in their study that wet removal through

94   transport in the PBL substantially reduced the transport efficiency of BC aerosols.   Here

95   we examine the effects of aging and wet removal during transport on the changes in BC

96   size distributions and mixing state, as well as concentrations, based on ground-based

97 measurements conducted at the same site in the spring of 2015 using a single particle soot

98 photometer (SP2) and an Aerosol Chemical Speciation Monitor (ACSM). We first

99 describe the meteorological characteristics of the East Asian region in the spring of 2015.

100 Then, we discuss the relative importance of the washout and rainout processes for the

101 removal of BC as well as the transport patterns of the East Asian outflow air masses in

102 spring. The loss of BC-containing particles for that period is investigated using a similar

103 approach to that used by Kanaya et al. (2016), and this is performed in connection with

104 the associated changes in BC microphysics and their relevance to the transport pathways.

105

106 **2. Experimental and data analysis**
107 **2.1. Atmospheric observations**

108 Continuous measurements of $PM_{2.5}$ and BC aerosols have been conducted at a remote

109 island, Fukue Island, since February 2009 (Kanaya et al., 2013; Ikeda et al., 2014). The

110 observation site is located at the Fukue Island Atmospheric Environment Monitoring

111 Station (32.75°N, 128.68°E, **Fig. 1**). The site is located in the northwest portion of

112 Fukue Island, approximately 20 km from the main residential area in the southeast. The

113 fine mode aerosols sampled at the site are mostly transported from areas beyond the island.

114 The enhanced concentrations of BC aerosols in Fukue Island can be mainly attributed to

115 long-range transport from the Asian continent, according to a previous study (Shiraiwa et

116 al., 2008) and an emission inventory work (**Fig. 1**, REAS ver. 2.1, Kurokawa et al., 2013).

117 We deployed an SP2 (Droplet Measurement Technologies, Inc., USA) for the analysis

118 of microphysical parameters of refractory BC (rBC, Petzold et al., 2013) from March 26,

119 2015 to April 14, 2015. The SP2 was calibrated before starting the ambient

120 measurements. The calibration protocol for our SP2 is described in Miyakawa et al.

121 (2016). Fullerene soot (FS, stock 40971, lot L20W054, Alfa Aesar, USA) particles were

122   used as a calibration standard for the SP2.   A differential mobility analyzer (Model 3081,

123   TSI Inc., USA) was used for preparing the monodisperse FS particles.   The analysis of

124   the calibration results suggests that the full width of half maxima (FWHM) was typically

125   30% of the modal incandescence signal intensity (S_{LII}) for the diameter range studied.

126   Note that the FWHM can be regarded as an upper limit to describe the resolving power

127   of rBC mass per particle using our SP2, because the combination of polydisperse size

128   distribution of FS particles and the transfer function of the DMA can broaden the

129   distributions of S_{LII} for the prepared FS particles.   The variations in the laser power were

130   within ±3% during the observation period, thus indicating that the fluctuations of laser

131   power did not largely affect the lower limit of the detectable rBC size using the SP2.

132   Mass equivalent diameter (MED) was derived from the rBC mass per particle (m_{pp}) with

133   an assumed particle density for BC (1800 kg m^{-3}, Bond and Bergstrom, 2006).   A large

134   diameter Nafion dryer (MD-700, Perma Pure, Inc., USA) was placed in front of the SP2

135   for drying the sample air without significant loss of the aerosol particles greater than 50

136   nm.   The dry air for MD-700 was generated by a heatless dryer (HD-2000, Perma Pure,

137   Inc., USA) and a compressor (2AH-23-M222X, MFG Corp., USA).   The relative

138   humidity of the sample air was less than 20% during the observation period.   The hourly

139   number/mass size distributions and hourly median values of shell (D_S) to rBC diameter

140   (D_{core}) ratios (D_S/D_{core}) for the selected D_{core} ranges were calculated.   The retrievals of

141   D_S from the light scattering signals measured by an avalanche photodiode and a position

142   sensitive detector (Gao et al., 2007) were performed using a time-resolved scattering cross

143   section method given by Laborde et al. (2012).   In this study, we quantified the D_S/D_{core}

144   ratios with a D_{core} range between 0.15 and 0.35 µm.   The maximum value of D_S/D_{core}

145   ratios analyzed is 4 in this study.   Retrived results suggest that almost all rBC particles

146   were not so thickly coated (for example, D_S/D_{core} ratios of ~2.5 at highest at D_{core} of 0.2

147   µm).   We also analyzed the microphysical parameters of rBC particles measured using

148   the SP2 in the early summer of 2014 at Yokosuka (35.32°N, 139.65°E, **Fig. 1**), located

149   near industrial sources along Tokyo Bay (Miyakawa et al., 2016).   These data sets were

150   used as a reference for the BC-containing particles in air masses strongly affected by

151   combustion sources.

152   Equivalent BC (EBC, Petzold et al., 2013) mass concentrations are continuously

153   measured at Fukue Island using two instruments; a continuous soot-monitoring system

154   (COSMOS; model 3130, Kanomax, Japan), and a multi-angle absorption photometer

155   (MAAP; MAAP5012, Thermo Scientific, Inc., USA).   The details of the air sampling

156   and intercomparisons for EBC measurements at Fukue Island have been described

157   elsewhere (Kanaya et al., 2013; 2016).   In this study, mass concentrations of EBC

158   measured using the COSMOS were evaluated by comparison with those of SP2-derived

159   rBC.   The intercomparison between SP2 and COSMOS will be briefly discussed below.

160   **Figure 2** depicts the correlation between COSMOS-EBC and SP2-rBC hourly mass

161   concentrations.   The unmeasured fraction of the rBC mass was corrected by

162   extrapolation of the lognormal fit for the measured mass size distributions, to the outsides

163   of the measurable D_{core} range (0.08-0.5 µm).   Note that the uncertainty with respect to

164   the unmeasured fraction of rBC mass was minor (<5%) in this study.   The linear

165   regression slope of the correlation between EBC and rBC was 0.88 (±0.03).   Uncertainty

166   with respect to the calibration was examined in an industrial region and found to be within

167   around 3% (Miyakawa et al., 2016).   The average discrepancy between EBC and rBC

168   was beyond the uncertainty of the calibration and was comparable to the uncertainty of

169   COSMOS (10%) as evaluated by Kondo et al. (2009).   While the validity of the

170 calibration standard, FS particles, has been evaluated only near source regions (Moteki

171 and Kondo, 2011; Miyakawa et al., 2016), the discrepancy can be partly attributed to the

172 differences in physicochemical properties between ambient BC in remote air and FS

173 particles.   Onsite calibration of the SP2 using ambient BC particles prepared by a

174 thermal denuder and particle mass classifier, such as an aerosol particle mass analyzer

175 (APM), is desirable for better quantification of the rBC mass based on the laser-induced

176 incandescence technique in remote areas.   Although we need to make further attempts

177 to evaluate SP2 in remote areas, this study indicated that SP2-rBC mass concentrations

178 agreed well with COSMOS-EBC within the uncertainty of COSMOS.   Therefore we

179 simply use "BC", instead of the EBC and rBC defined depending upon the measurement

180 techniques.   We analyzed the COSMOS data for the BC mass concentrations, and the

181 SP2 data for the BC microphysics.

182 The chemical composition of non-refractory submicron aerosols was measured using

183 an Aerodyne Aerosol Chemical Speciation Monitor (ACSM, Aerodyne, Inc., USA.)

184 placed in an observatory container at Fukue Island during the observation period.   The

185 details of the ACSM at Fukue Island have been described in Irei et al. (2014).   The

186 collection efficiency (CE) of the ACSM was assumed to be 0.5 for this period (Yoshino

187 et al., 2016).   We considered sulfate (SO_4^{2-}) ions as a major non-BC material and one of

188 the most important secondary aerosols in East Asia (Takami et al., 2007) for the data

189 interpretation.   The fact that SO_4^{2-} is produced in the cloud phase as well as in the gas

190 phase is beneficial for interpreting temporal changes in SO_4^{2-} concentration associated

191 with the wet removal processes.   We also analyzed other non-refractory components

192 such as nitrate (NO_3^-), ammonium (NH_4^+), and organic matter (OM).   During the period

193 April 1 -7, 2015, the critical orifice of the inlet assembly of the ACSM became clogged.

194   ACSM-derived SO_4^{2-}, NO_3^-, NH_4^+, and OM (ACSM- SO_4^{2-}, -NO_3^-, -NH_4^+, and -OM) for

195   this period was not used in the analysis.

196   Two high volume air samplers (HV500F, Sibata Scientific Technology, Ltd., Japan)

197   were deployed on the rooftop of the observatory container.   The sampling flow rate for

198   both samplers was 500 liters per minute (lpm).   Air sampling was carried out for 21 h

199   (from 10:00 AM to 7:00 AM) on a 110-mm pre-combusted (900°C for 3 h) quartz filter

200   (QR-100, Advantec Toyo Kaisha Ltd., Japan).   Both have a $PM_{2.5}$ impactor for

201   classifying the particle size.   One impaction plate was coated with vacuum grease

202   (HIVAC-G, Shin-Etsu Chemical Co., Ltd., Japan) to minimize the impact of coarse mode

203   particles on the chemical analysis of fine mode particles such as radiocarbon analysis,

204   and a pre-combusted quartz fiber filter with slits was set on another impaction plate to

205   collect the coarse particles.   Water soluble ions were analyzed using ion chromatography

206   (IC, Dionex ICS1000, Thermo Fisher Scientific K.K., Japan).   The results from the

207   chemical analysis of filter samples are not discussed in this study in detail.   We only

208   used the mass concentration of SO_4^{2-} (IC-SO_4^{2-}) in this study to evaluate the uncertainty

209   in relation to CE of the ACSM, and to analyze the temporal variations during the period

210   when the ACSM-SO_4^{2-} data were not available (April 1-7, 2015).

211   The carbon monoxide (CO) mixing ratio was also continuously measured using a

212   nondispersive infrared (NDIR) CO monitor (model 48C, Thermo Scientific, Inc., USA).

213   Details of the CO measurements including the long-term variations in sensitivity and zero

214   level are discussed elsewhere (Kanaya et al., 2016).

215

216   **2.2. Enhancement ratio of BC and SO_4^{2-} to CO as an indicator of the transport and**

217   **transformation of aerosol particles**

218   In order to quantify the extent of the removal of BC, we calculated the hourly

219   enhancement ratio of BC mass concentrations to CO mixing ratios (ΔBC/ΔCO) against

220   the East Asian background air concentrations as follows:

221

222      $$\frac{\Delta BC}{\Delta CO} = \frac{[BC] - [BC]_{bg}}{[CO] - [CO]_{bg}},$$ (1)

223

224   where [BC] and [CO] are measured hourly concentrations of the BC and CO respectively,

225   and $[BC]_{bg}$ and $[CO]_{bg}$ are their estimated background concentrations.   Here we assumed

226   that $[BC]_{bg}$ is zero (Oshima et al., 2012).   The background concentration of CO during

227   the analysis period (March 11 – April 14, 2015) was calculated by averaging the

228   concentrations lower than the 5th percentile (120 ppb).   The validity of this value is

229   discussed in the supporting information (S.I.).

230   Relative changes in SO_4^{2-} to CO were also analyzed using the linear regression slopes

231   of their correlation in this study.   We did not calculate their hourly values, because it was

232   difficult to determine the background concentration of SO_4^{2-}.   The use of CO as a tracer

233   of sulfur compounds in East Asia was validated by Koike et al. (2003).   Although sulfur

234   dioxide (SO_2), which is a major precursor of anthropogenic SO_4^{2-}, does not always share

235   the emission sources with CO, the special distributions of SO_2 emissions is similar to

236   those of CO emissions in East Asia (Koike et al., 2003; Kurokawa et al., 2013).

237   Analyzing the increase or decrease in the slopes of the SO_4^{2-}-CO correlation is beneficial

238   to the investigation of the formation and removal processes for SO_4^{2-}.   Especially, the

239   aqueous-phase reaction of SO_4^{2-} in clouds is discussed using this parameter.

240

2.3. Meteorological field analysis

We used the 6-hourly meteorological data, with a resolution of $1°$ in terms of the latitude and longitude, from the National Centers for Environmental Prediction (NCEP) Final (FNL) operational global analysis; and daily precipitation data, with a resolution of $1°$ in terms of the latitude and longitude, from the Global Precipitation Climatology Project (GPCP) data set (Huffman et al., 2001). We analyzed these data sets to investigate the general features of the meteorological field in East Asia during the observation period.

2.4. Backward trajectory analysis

We calculated backward trajectories from the observation site to elucidate the impact of the Asian outflow. Three-day backward trajectories from the observation site (the starting altitude was 0.5 km) were calculated every hour using the National Oceanic and Atmospheric Administration (NOAA) Hybrid Single-Particle Lagrangian Integrated Trajectory model (Draxler and Rolph, 2012; Rolph, 2012) with the meteorological data sets (NCEP's Global Data Assimilation system, GDAS). In this study, the residence time over specific source regions was used as an indicator of their impacts on the observed air masses. We defined five domains for assessing the impact over the Asian continent; Northeast China (NE), Korea (KR), Central North China (CN), Central South China (CS), and Japan (JP) (**Fig. 1**). The period when air masses passed over the domains NE, KR, CN, and CS at least for one hour is defined as that of "continental outflow". The impacts of precipitation on the observed air masses were assessed by a parameter referred to as the "Accumulated Precipitation along Trajectory" (APT, Oshima et al., 2012). In this

264   study, we calculated the APT values by integrating the amount of hourly precipitation in

265   the Lagrangian sense along each 3-day back trajectory of the sampled air masses.   The

266   hourly variations of APT were merged into the observed gas and aerosol data sets.

267

268   **3.   Results and discussion**

269   **3.1.   The meteorological field in the spring of 2015**

270   The mean meteorological field during the observation period (March 11−April 14,

271   2015) is discussed for the purpose of characterizing the general features of the wind flow

272   and precipitation in this region. The migrating anticyclone and cyclone were observed

273   during this period, which is typically dominant in spring over East Asia (Asai et al., 1988).

274   We here only briefly describe the meteorological fields (wind flow and precipitation) in

275   the following.   **Figure 3a** shows the mean sea level pressure (SLP) and mean horizontal

276   winds at the 850 hPa level in East Asia during the observation period.   The mean

277   equivalent potential temperature (θe) and the meridional moisture transport at the 850 hPa

278   level during the same period are also shown in **Figure 3b**.   The mid-latitude region (35-

279   50°N, 120-140°E) was under the influence of a modest monsoonal northwesterly flow,

280   which advected cold, dry air from the continent to the observation area.   The subtropical

281   region (20°-30°N, 110°-130°E) was under the influence of a persistent southwesterly flow,

282   part of which was conversing into the observation area (30°-35°N), and this flow was

283   confluent with the northwesterlies from the continent.   The low-level southerly flow

284   advected warm, moist air into the observation area to sustain a large amount of

285   precipitation (**Fig. 4a**).

286   **Figure 3c** shows the temporal variations in surface pressure and precipitable water at

287   the observation site.   The surface pressure is well anti-correlated with the precipitable

288   water.   During the observation period, migratory cyclones and anticyclones occurred

289 occasionally (3 times each).   The occurrence of migratory cyclones advected moist air,

290 which could have contributed to the wet removal of BC during transport in the PBL.   In

291 contrast, the occurrence of anticyclones advected dry air, which could have contributed

292 to the efficient transport of BC from the source regions.

293 **Figure 4a** depicts the mean precipitation over East Asia during the observation period.

294 Mean precipitation showed a latitudinal gradient over eastern China and the Yellow Sea

295 and East China Sea region (i.e., increasing precipitation from south to north), and these

296 results suggest that transport pathways can greatly affect the wet removal of aerosols.

297 The APT was compared with the averaged latitude of each trajectory for 48 h backwardly

298 from the time of -24 h (Lat$_{ORIG}$) (**Fig. 4b**), which can be interpreted as an indicator of the

299 latitudinal origin of the air masses arriving at Fukue Island.   The high APT values

300 corresponded to the air masses that originated from the southern regions (20º-40ºN).

301 The data points are colored according to the maximum RH values along each backward

302 trajectory (RH$_{max}$).   The lower relative humidty (RH$_{max}$) were observed in the air masses

303 with low APT values that originated from northern regions (30º-50ºN).   These air mass

304 characteristics were consistent with the mean precipitation field (**Fig. 4a**).   Some of the

305 data points showed high values of RH$_{max}$ (~100%) when their APT was almost zero.

306 These data probably correspond to the air masses that experienced cloud processes not

307 associated with precipitation.   Possible effects of cloud processes without precipitation

308 on the removal of aerosol particles during transport will be discussed using these data

309 points in the following section.

310

311 **3.2. Removal processes of fine aerosol particles**

312 In this study, the removal processes including dry deposition and washout were

313 considered to be minor. The dry deposition in this region has already been evaluated by

314 Kanaya et al. (2016). The washout is dependent on the precipitation intensity and rain

315 drop size as well as the particle size range. We quantitatively investigated the relative

316 importance of rainout to washout in this study. The removal rates of submicron

317 accumulation mode particles through the washout (Λ_{accum}) was estimated to be $\sim 1 \times 10^{-3}$

318 h^{-1} ($0.5\text{-}2 \times 10^{-3}$ h^{-1}) using a parametrization given by Wang et al. (2014) and the average

319 precipitation intensity along the trajectories (0.78 ± 0.6 mm h^{-1}) as an input to the

320 parameterization. The possible uncertainties in this estimation are derived from the

321 discrepancies in Λ_{accum} the removal rates between the parameterization and some

322 experimental results (Wang et al., 2014). The values of Λ_{accum} can be underestimated by

323 an order of magnitude by using the parameterization, which is however overly pessimistic.

324 The temporal duration in rain along trajectories for air masses with the APT greater than

325 0 mm was 10 (± 8) hours on average. These values can be used for the estimation of the

326 removed fraction of submicron aerosols through the washout process. The average

327 fraction of submicron aerosols removed was 1% (+2.59%/-0.9%). Even though we took

328 into account the uncertainties for estimating Λ_{accum}, it was found that the washout process

329 did not play a major role in the removal of BC in East Asian outflow.

330

331 **3.3. Temporal variations in aerosols and CO**

332 Temporal variations in the concentrations of BC (measured using COSMOS and SP2),

333 SO_4^{2-} (measured using ACSM and IC), NO_3^-, OM, and CO are shown in **Figure 5**.

334 ACSM-SO_4^{2-} generally agreed well with IC-SO4, thus indicating that the assumed CE

335 (0.5) was valid for the observation period. As NO_3^- and SO_4^{2-} were almost fully

336 neutralized by NH_4^+, we assumed their chemical forms were ammonium salts. In

337 general, BC, SO_4^{2-}, and OM were positively correlated with CO at Fukue Island, and these

338 results illustrate the impact of continental outflow affected by incomplete combustion

339 sources on aerosol mass concentrations.   The mean chemical composition of fine

340 aerosols during the observation period was listed in **Table 1**.   Ammonium sulfate and

341 OM were abundant components.   **Figure 5** also includes the temporal variations in the

342 fractional residence time over the selected region defined in section 2.4 (top panel).   The

343 CO concentrations were typically enhanced for the period with the higher contributions

344 of CN and CS.   A previous study suggested that the majority of SO_4^{2-} aerosols were

345 formed in less than around 1.5 days after the air masses left the Chinese continent (Sahu

346 et al., 2009).   Kanaya et al. (2016) showed that the typical transport time of continental

347 outflow air masses at Fukue Island was around 1-2 days in spring.   The positive

348 correlation of SO_4^{2-} and CO suggests that the secondary formation of SO_4^{2-} through

349 transport was significant during the observation period.   The structure and composition

350 of fine aerosols in East Asian outflow were analyzed by using a secondary ion mass

351 spectrometer in a previous study (Takami et al., 2013).   They suggest that SO_4^{2-} and OM

352 are constituents in the coating of almost all BC-containing particles.   Hence we

353 concluded that ammonium sulfate and OM contributed to the growth of BC-containing

354 particles.   The period with the APT > 3 mm is highlighted by light blue in **Figure 5** to

355 show the impact of wet removal on the transport of BC and SO_4^{2-} aerosols.   The

356 maximum concentrations of aerosols and CO were observed on the morning of March 22

357 (Ep.1) under the influence of the anticyclone (corresponding to the trajectories colored

358 red in **Fig. 4a**) when the APT values were almost zero.   In contrast, aerosol

359 concentrations did not increase with CO in the period from the evening of April 5 to the

360 morning of April 6 (Ep.2) under the influence of the migratory cyclone (corresponding to

361   the trajectories colored black in **Fig. 4a**), when the APT was greater than 10 mm.

362

363   **3.4. Correlation of BC, SO_4^{2-}, and CO**

364   **Figures 6a** and **6b** show scatter plots of CO with BC and SO_4^{2-}, respectively.   Positive

365   correlation of BC and SO_4^{2-} with CO was clearly found in air masses with low APT values.

366   The linear regression was performed to the data points with the APT higher than 15 mm

367   for BC-CO and SO_4^{2-}-CO.   Note that the linear regression slope for BC-CO was

368   determined by forcing through the background concentrations of BC (0 μg m^{-3}) and CO

369   (120 ppb).   The slopes of the fitted lines were 1.4 and 9.8 ng m^{-3} ppb^{-1} for BC-CO and

370   SO_4^{2-}-CO, respectively, were close to the lower envelopes of the correlations.   It is

371   evident from these scatter plots that the relative enhancements of BC and SO_4^{2-} to CO

372   were mainly affected by the APT.   Kanaya et al. (2016) found that the estimated

373   emission ratios of BC to CO over the East Asian continent ranged from 5.3 ($\pm$2.1) to 6.9

374   ($\pm$1.2) ng m^{-3} ppb^{-1}, slightly depending on the origin of the air masses (this range is

375   overlaid on **Fig. 6a**). ΔBC/ΔCO observed in the PBL over the Yellow Sea during the

376   same season was 6.2 ng m^{-3} ppb^{-1} (Kondo et al., 2016).   The data points with ΔBC/ΔCO

377   in these ranges show low APT values (less than or ~1 mm).   Wet removal (rainout) was

378   one of the most important controlling factors on the transport efficiency of BC in this

379   region during the observation period.   The use of the ΔBC/ΔCO ratios is feasible for

380   examining the wet removal of BC during the observation period.

381   The cloud processes of aerosol particles not associated with precipitation can also

382   reduce the slope of their correlation.   However, no decreasing tendency of BC/CO and

383   SO_4^{2-}/CO slopes against RH_{max} when APT was zero was found during the observation

384   period (data not shown).   The SO_4^{2-}/CO slopes with the APT values of zero were

385 analyzed as a function RH_{max} (**Figure 6b**), and these varied from 30.7 to 44.1 ng m^{-3} ppb^{-}

386 ^{1} under the conditions without (RH_{max} <50%) and with (RH_{max} >80%) cloud impacts,

387 respectively.   The SO_4^{2-}/CO slope increased with RH_{max} when the APT was zero, thus

388 suggesting that aqueous phase formation and subsequent droplet evaporation partly

389 contributed to the mass concentrations of SO_4^{2-} observed at Fukue Island.   Therefore,

390 the changes in the SO_4^{2-}/CO correlation were controlled largely by the rainout process

391 and weakly by aqueous-phase formation during transport.

392

393 **3.5. Changes in fine aerosol compositions**

394 Chemical compositions of fine aerosols were investigated in terms of the APT and

395 RH_{max}.   Four cases are selected here, namely (1) APT of zero (no precipitation), (2) APT

396 of zero with RH_{max} <50% (no precipitation without cloud impacts), (3) APT of zero with

397 RH_{max} >80% (no precipitation with cloud impacts), and (4) APT >15 mm (heavily

398 affected by wet removal).   The results are summarized in **Table 1**.   Ammonium sulfate

399 and OM were dominant in all cases.   The relative changes in chemical compositions of

400 fine aerosol particles were within around 10%.   The relative contributions of ammonium

401 sulfate in the cases (3) and (4) increased from the average, indicating that cloud processes

402 affected the relative abundance of ammonium sulfate.   The contributions of OM in the

403 case (2) increased from the average.   The formation of secondary OM can be significant

404 under dry conditions during transport.   Detailed mass spectral analyses of OM and

405 cloud-phase formation of OM in East Asia are beyond the scope of this study, and they

406 are not discussed in this study.   The former issue has been investigated by previous

407 studies (e.g., Irei et al., 2014; Yoshino et al., 2016).

408

409 **3.6. Changes in microphysical parameters of BC-containing particles associated**

	with wet removal

411	Number and mass size distributions of BC classified by the values of ΔBC/ΔCO are

412	shown in **Figures 7a** and **7b**, respectively. When ΔBC/ΔCO values in continental

413	outflow air masses were greater than 3 ng m^{-3} ppb^{-1} (within the range of the BC/CO

414	emission ratios given by Kanaya et al. 2016), these air masses are defined as "outflow

415	without BC loss". These air masses originated mainly from CN via KR and NE. When

416	ΔBC/ΔCO values of continental outflow air masses are less than 1 ng m^{-3} ppb^{-1}, the air

417	masses were defined as "outflow with BC loss". Considering the typical emission ratios

418	of BC to CO (6-7 ng m^{-3} ppb^{-1}; Kanaya et al., 2016), transport efficiency for the "outflow

419	with BC loss" air masses can be estimated to be less than ~17%. These air masses

420	originated mainly in CS. The low and high APT values for "outflow without BC loss"

421	and "outflow with BC loss" air masses, respectively, gave us confidence in the validity

422	of our classification as discussed in the previous section. As a reference for emission

423	sources ("source"), the average size distributions of BC in a Japanese industrial area (see

424	section 2.1, Miyakawa et al., 2016) are shown in **Figure 7**. The statistics of the size

425	distributions are summarized in **Table 2**. Observed differences in the size distributions

426	between source and outflow were generally consistent with previous studies (Schwarz et

427	al., 2010). Air mass aging leads to the growth of BC-containing particles. Number-

428	size distributions of BC largely varied in the size range less than 0.1 µm (**Fig. 7a**). In

429	outflow air masses, such small BC-containing particles were scavenged by larger particles

430	in the coagulation process during transport. The washout process can also affect the

431	BC-containing particles in the smaller size range (<0.1 µm). The peak diameter of mass

432	(number) size distributions of BC became larger, from 0.16 (0.06) µm to 0.18-0.2 (0.09-

433	0.1) µm, between source and outflow. The BC-containing particles have systematically

434   different size distributions in outflow air masses with and without BC loss, indicating that

435   the BC loss process also affected the size distributions.   The peak diameter of BC

436   number and mass size distributions in outflow air masses with BC loss was slightly lower

437   than that for air masses without BC loss.   The changes in the peak diameter as a function

438   of $\Delta BC/\Delta CO$ ratios are shown in **Figure 7c**.   The observed changes in the diameter or

439   mass per particle were clear and were beyond the uncertainties (see section 2.1).

440   **Figure 8** depicts the probability density of the D_S/D_{core} ratio for the BC size of 0.2

441   (± 0.02) µm for source and outflow air masses.   The modal values of the D_S/D_{core} ratio

442   were systematically changed with air mass aging and BC loss (wet removal).   The

443   condensation of inorganic and organic vapors on BC-containing particles during transport

444   can account for the increase in the D_S/D_{core} ratio, as discussed in previous studies (e.g.,

445   Shiraiwa et al., 2008; Subramanian et al. 2010).   As discussed earlier, the results of this

446   study suggested that SO_4^{2-} and OM substantially contributed to the increase in the D_S/D_{core}

447   ratio.   In outflow air masses with BC loss, modal values of the D_S/D_{core} ratio were clearly

448   lower than those in outflow without BC loss.   Furthermore, it is indicated that the wet

449   removal process also affected the coating thickness distributions for the BC sizes in the

450   range 0.15-0.35 µm (**Table 2**).   It should be noted that the coating of BC-containing

451   particles is not always thick in remote regions, and that the D_S/D_{core} ratio distributions, as

452   well as size distributions, can be affected by the wet removal process during transport in

453   the PBL.

454

455   **3.7. Discussion**

456   Not only in-cloud scavenging of BC-containing particles but also subsequent

457   precipitation (i.e., the rainout process) can account for the changes in the microphysical

458 parameters of BC detected in this study.   Our results show a decrease of both the peak

459 diameter of the BC mass size distribution, and the modal value of the D_S/D_{core} ratios in

460 relation to the rainout.   The observed evidence implies that there can be the selective

461 removal of large and water-soluble BC-containing particles during transport in the PBL.

462 The Köhler theory suggests that a lower super saturation is needed for the large and highly

463 water-soluble particles, and this can qualitatively account for the observed changes in the

464 BC microphysics.

465   Note that the magnitude of the change in the BC size distributions in the PBL (~0.02

466 µm (~2-2.5 fg)) shown in **Figure 7c** is smaller than that observed in air masses uplifted

467 from the PBL to the FT, in association with wet removal (~0.04 µm (~3 fg), Fig 2 of

468 Moteki et al., 2012) at a similar level of transport efficiency (<~20%).   Although the

469 shape of mass size distributions soon after the rainout processes can be distorted by the

470 droplet activation of larger aerosol particles, the observed mass size distributions were

471 well fitted by a log-normal function (**Fig. 7b**).   **Figure 8** showed the existence of BC-

472 containing particles with the D_S/D_{core} ratios higher than 1.2 even in outflow air masses

473 with BC loss that are expected to readily act as CCN.   Air masses sampled at the ground

474 level would be affected by turbulent mixing of those near the clouds around the top of the

475 PBL and those in cloud-free conditions at below-cloud levels.   On the other hand, most

476 air masses sampled by aircraft measurements in the FT would experience the cloud

477 processes during upward transport from the PBL.   Mixing of air masses in the PBL

478 suggests that they partially experience the in-cloud scavenging processes.   The aging

479 (e.g., coagulation) of aerosols particles through the transport (i.e., around ~1 day) after

480 the wet removal events can also lead to the further modification of the particle size and

481 mixing state distributions which have been affected by cloud processes.   The

482 suppression of changes in the microphysical properties of BC-containing particles during

483 transport in the PBL can be related to these factors.   More quantitative assessments of

484 the impacts of these factors on the observed features should be performed using a model

485 which has a function to resolve the mixing state of aerosol particles (e.g., Matsui et al.,

486 2013).

487   The transport pathways of the continental outflow air masses are horizontally and

488 vertically variable in spring in East Asia because of the frequent alternate

489 cyclone/anticyclone activities in spring (Asai et al., 1988).   Oshima et al. (2013)

490 examined the three-dimensional transport pathways of BC over East Asia in spring and

491 showed that the PBL outflow through which BC originating from China was advected by

492 the low-level westerlies without uplifting out of the PBL was one of the major pathways

493 for BC export from continental East Asia to the Pacific, thus supporting the general

494 features of microphysical properties of BC in continental outflow obtained by this study.

495 Mori et al. (2014) measured the seasonal variations in BC wet deposition fluxes at another

496 remote island in Japan (Okinawa, ~500 km south of Fukue Island), and revealed their

497 maxima in spring, which were consistent with the seasonal variations in the cyclone

498 frequencies.   It has been suggested that BC-containing particles were efficiently

499 activated to form cloud droplets in the continental outflow air masses, especially from the

500 CS region, and can affect the cloud physicochemical properties in spring in East Asia, as

501 indicated by Koike et al. (2012).   As the results from this study are based on the

502 observations during a limited length of time, it would be worthwhile to further investigate

503 the possible connections of the variabilities in BC microphysical properties with

504 meteorological conditions to provide useful constraints on more accurate evaluations

505 climatic impacts of BC-containing particles in this region (Matsui, 2016).

506

4. Conclusions

Ground-based measurements of BC were performed near an industrial source region and at a remote island in Japan. We have reported the temporal variations in the transport and the microphysics of the BC-containing particles, measured using COSMOS, SP2, and ACSM. The impacts of air mass aging upon the growth of BC-containing particles were examined by comparing the ground-based observations between the near-source and remote island sites. $\Delta BC/\Delta CO$ was used as an indicator of the transport efficiency of BC, because it was controlled mainly by rainout during transport in the PBL. The BC size and coating increased during transport from the near-source to the outflow regions on the timescale of 1-2 days when the rainout during transport was negligible. SO_4^{2-} aerosol was secondarily formed both in the gas- and cloud-phase during transport, and it contributed to the significant increase in the coating materials of BC (i.e., it enhanced the whole size and water-solubility of BC-containing particles). Decreases in the peak diameter of mass size distributions (~0.01 µm) and modal D_S/D_{core} ratios (~0.4 for BC of 0.2 µm) of BC-containing particles were observed in air masses substantially affected by rainout. The observed evidences for the selective removal of large and water-soluble BC-containing particles was qualitatively consistent with the Köhler theory; however the values were not as large as those found in air masses uplifted from the PBL to the FT in East Asia associated with precipitation. The mixing of below-cloud and in-cloud air masses in the PBL would result in suppression of the degree of changes in BC microphysical parameters by cloud processes. This study indicates (1) that the changes (sign and degree) in BC microphysics can be affected by how the air masses are transported and (2) that the observed selective removal of large and water-soluble BC-

530 containing particles in East Asia can be expected to be significant in the PBL as well as

531 in the FT in East Asia.

532

533

534 **Acknowledgments**

535   This study was supported by the Environment Research and Technology

536 Development Fund (S7, S12, and 2-1403) of the Ministry of Environment, Japan, and

537 the Japan Society for the Promotion of Science (JSPS), KAKENHI Grant numbers

538 JP26550021, JP26701004, JP26241003, JP16H01772, and JP16H01770, and was

539 partially carried out in the Arctic Challenge for Sustainability (ArCS) Project.   The

540 authors would like to thank N. Moteki at the University of Tokyo for assistance with the

541 SP2 calibrations.   M. Kubo, T. Takamura, and H. Irie (Chiba University) are also

542 acknowledged for their support at the Fukue-Island Atmospheric Environment

543 Monitoring Station.

544

545 **References**

546 Asai, T., Y. Kodama, and J.-C. Zhu, Long-term variations of cyclone activities in East

547   Asia, Adv. Atmos. Sci., 5, 149−158, 1988.

548 Bond, T. C. and R. W. Bergstrom, Light Absorption by Carbonaceous Particles: An

549   Investigative Review, Aerosol Sci. Technol., 40, 27-67, 2006.

550 Bond, T., et al.. Bounding the role of black carbon in the climate system: a scientific

551   assessment. J. Geophys. Res., 118, 5380–5552, doi:10.1002/jgrd.50171, 2013.

552 Draxler, R. R., and Rolph, G. D., HYSPLIT (HYbrid Single-Particle Lagrangian

553   Integrated Trajectory) Model access via NOAA ARL READY Website

554   (http://ready.arl.noaa.gov/ HYSPLIT.php), NOAA Air Resources Laboratory, Silver

555   Spring, Md., 2012.

556   Gao, R. S., Schwarz, J. P., Kelly, K. K., Fahey, D. W., Watts, L. A., Thompson, T. L.,

557   Spackman, J. R., Slowik, J. G., Cross, E. S., Han, J. H., Davidovits, P., Onasch, T. B.,

558   and Worsnop, D. R., A novel method for estimating light-scattering properties of soot

559   aerosols using a modified single-particle soot photometer, Aerosol Sci. Tech., 41,

560   125–135, 2007.

561   Hinds, W. C., Aerosol Technology: Properties, Behavior, and Measurement of Airborne

562   Particles, Wiley-Interscience, New York, 1999.

563   Huffman, G.J., R.F. Adler, M. Morrissey, D.T. Bolvin, S. Curtis, R. Joyce, B McGavock,

564   and J. Susskind, Global Precipitation at One-Degree Daily Resolution from Multi-

565   Satellite Observations. *J. Hydrometeor*., 2, 36-50, 2001.

566   Ikeda, K., K. Yamaji, Y. Kanaya, F. Taketani, X. Pan, Y. Komazaki, J. Kurokawa, and T.

567   Ohara, Sensitivity Analysis of Source Regions to PM2.5 Concentration at Fukue

568   Island, Japan, J. Air Waste Manage. Assoc., doi:10.1080/10962247.2013.845618,

569   2014.

570   Irei, S., A. Takami, M. Hayashi, Y. Sadanaga, K. Hara, N. Kaneyasu, K. Sato, T. Arakaki,

571   S. Hatakeyama, H. Bandow, T. Hikida, and A. Shimono, Transboundary Secondary

572   Organic Aerosol in Western Japan Indicated by the δ13C of Water-Soluble Organic

573   Carbon and the m/z 44 Signal in Organic Aerosol Mass Spectra, Environ. Sci.

574   Technol., 48, 6273-6281, 2014.

575   Kanaya, Y., F. Taketani, Y. Komazaki, X. Liu, Y. Kondo, L. K. Sahu, H. Irie, and H.

576   Takashima, Comparison of black carbon mass concentrations observed by Multi-

577   Angle Absorption Photometer (MAAP) and Continuous Soot-Monitoring System

578   (COSMOS) on Fukue Island and in Tokyo, Japan, Aerosol Sci. Technol., 47, 1-10,

579   2013.

580   Kanaya, Y., X. Pan, T. Miyakawa, Y. Komazaki, F. Taketani, I. Uno, and Y. Kondo,

581   Long-term observations of black carbon mass concentrations at Fukue Island, western

582   Japan, during 2009-2015: Constraining wet removal rates and emission strengths

583   from East Asia, Atmos. Phys. Chem., 16, 10689-10705, doi:10.5194/acp-16-10689-

584   2016, 2016.

585   Koike, M., et al., Export of anthropogenic reactive nitrogen and sulfur compounds from

586   the East Asia region in spring, J. Geophys. Res., 108(D20), 8789,

587   doi:10.1029/2002JD003284, 2003.

588   Koike, M., N. Takegawa, N. Moteki, Y. Kondo, H. Nakamura, K. Kita, H. Matsui, N.

589   Oshima, M. Kajino, and T. Y. Nakajima, Measurements of regional-scale aerosol

590   impacts on cloud microphysics over the East China Sea: Possible influences of warm

591   sea surface temperature over the Kuroshio ocean current, J. Geophys. Res., 117,

592   D17205, doi:10.1029/2011JD017324, 2012

593   Kondo, Y., L. Sahu, N. Moteki, F. Khan, N. Takegawa, X. Liu, M. Koike and T.

594   Miyakawa, Consistency and Traceability of Black Carbon Measurements Made by

595   Laser-Induced Incandescence, Thermal-Optical Transmittance, and Filter-Based

596   Photo-Absorption Techniques, Aerosol Sci. Technol., 45, 295-312, 2009

597   Kondo, Y., N. Moteki, N. Oshima, S. Ohata, M. Koike, Y. Shibano, N. Takegawa, and K.

598   Kita, Effects of Wet Deposition on the Abundance and Size Distribution of Black

599   Carbon in East Asia, J. Geophys. Res. Atmos., 121, doi:10.1002/2015JD024479,

600   2016

601   Kurokawa, J., T. Ohara, T. Morikawa, S. Hanayama, G. Janssens-Maenhout, T. Fukui, K.

602   Kawashima, and H. Akimoto, Emissions of air pollutants and greenhouse gases over

603   Asian regions during 2000-2008: Regional Emission inventory in ASia (REAS)

604   version 2, Atmos. Chem. Phys., 13, 11019-11058, doi:10.5194/acp-13-11019-2013,

605   2013

606   Kuwata, M., Y. Kondo, M. Mochida, N. Takegawa, and K. Kawamura, Dependence of

607   CCN activity of less volatile particles on the amount of coating observed in Tokyo, J.

608   Geophys. Res., 112, D11207, doi:10.1029/2006JD007758, 2007

609   Kuwata, M., Y. Kondo, and N. Takegawa, Critical condensed mass for activation of black

610   carbon as cloud condensation nuclei in Tokyo, J. Geophys. Res., 114, D20202,

611   doi:10.1029/2009JD012086, 2009

612   Laborde, M., Mertes, P., Zieger, P., Dommen, J., Baltensperger, U., and Gysel, M.,

613   Sensitivity of the Single Particle Soot Photometer to different black carbon types,

614   Atmos. Meas. Tech., 5, 1031–1043, doi:10.5194/amt-5-1031-2012, 2012

615   Lawrence, M., T. M. Butler, J. Steinkamp, B. R. Gurjar, and J. Lelieveld, Regional

616   pollution potentials of megacities and other major population centers, Atmos. Chem.

617   Phys., 7, 3969-3987, 2007

618   Liu, J., S. Fan, L. W. Horowitz, and H. Levy II, Evaluation of factors controlling long-

619   range transport of black carbon to the Arctic, J. Geophys. Res., 116, D04307,

620   doi:10.1029/2010JD015145, 2011

621   Mari, X., et al., Effects of soot deposition on particle dynamics and microbial processes

622   in marine surface waters, Global Biogeochem. Cycles, 28, 662–678,

623   doi:10.1002/2014GB004878, 2014.

624   Matsui, H., M. Koike, Y. Kondo, N. Moteki, J. D. Fast, and R. A. Zaveri, Development

625   and validation of a black carbon mixing state resolved three-dimensional model:

626   Aging processes and radiative impact, J. Geophys. Res. Atmos., 118, 2304-2326,

627   doi:10.1029/2012JD018446, 2013.

628   Matsui, H., Black carbon simulations using a size- and mixing-state-resolved three-

629   dimensional model: 1. Radiative effects and their uncertainties, J. Geophys. Res.

630   Atmos., 121, 1793–1807, doi:10.1002/2015JD023998, 2016.

631   McMeeking, G. R., N. Good,   M. D. Petters, G. McFiggans, and H. Coe, Influences on

632   the fraction of hydrophobic and hydrophilic black carbon in the atmosphere, Atmos.

633   Chem. Phys., 11, 5099-5112, 2011.

634   Miyakawa, T., Y. Kanaya, Y. Komazaki, F. Taketani, X. Pan, M. Irwin, J. Symonds,

635   Intercomparison between a single particle soot photometer and evolved gas analysis

636   in an industrial area in Japan: Implications for the consistency of soot aerosol mass

637   concentration measurements, Atmos. Environ., 127, 14-21, 2016.

638   Mori, T., Y. Kondo, S. Ohata, N. Moteki, H. Matsui, N. Oshima, and A. Iwasaki, Wet

639   deposition of black carbon at a remote site in the East China Sea, J. Geophys. Res.

640   Atmos., 119, 10,485–10,498, doi:10.1002/2014JD022103, 2014.

641   Moteki, N. and Y. Kondo, Depndence of laser-induced incandescence on physical

642   properties of black carbon aerosols: measurements and theoretical interpretation,

643   Aerosol Sci. Technol., 44, 663-675, 2011.

644   Moteki, N., Y. Kondo, N. Oshima, N. Takegawa, M. Koike, K. Kita, H. Matsui, and M.

645   Kajino, Size dependence of wet removal of black carbon aerosols during transport

646   from the boundary layer to the free troposphere, Geophys. Res. Lett., 39, L13802,

647   doi:10.1029/2012GL052034, 2012.

648   Oshima, N., M. Koike, Y. Zhang, Y. Kondo, N. Moteki, N. Takegawa, and Y. Miyazaki,

649   Aging of black carbon in outflow from anthropogenic sources using a mixing state

650   resolved model: Model development and evaluation, J. Geophys. Res., 114, D06210,

651   doi:10.1029/2008JD010680, 2009.

652   Oshima, N., et al., Wet removal of black carbon in Asian outflow: Aerosol Radiative

653   Forcing in East Asia (A-FORCE) aircraft campaign, J. Geophys. Res., 117, D03204,

654   doi:10.1029/2011JD016552, 2012.

655   Oshima, N., and M. Koike, Development of a parameterization of black carbon aging for

656   use in general circulation models, Geophys. Model. Dev., 6, 263-282, 2013.

657   Oshima, N., M. Koike, Y. Kondo, H. Nakamura, N. Moteki, H. Matsui, N. Takegawa,

658   and K. Kita, Vertical transport mechanisms of black carbon over East Asia in spring

659   during the A-FORCE aircraft campaign, J. Geophys. Res. Atmos., 118, 13,175–

660   13,198, doi:10.1002/2013JD020262, 2013.

661   Petzold, A., J.A. Ogren, M., Fiebig, S. M. Li, U. Bartensperger, T. Holzer-Popp, S. Kinne,

662   G. Pappalardo, N. Sugimoto, C. Wehrli, A. Wiedensohler, and X. Y. Zhang,

663   Recommendations for reporting "black carbon" measurements, Atmos. Chem. Phys.

664   13, 8365-8379, 2013.

665   Rolph, G. D., Real-time Environmental Applications and Display system (READY)

666   Website (http://ready.arl.noaa.gov). NOAA Air Resources Laboratory, Silver Spring,

667   Md., 2012.

668   Sahu, L. K., Y. Kondo, Y. Miyazaki, M. Kuwata, M. Koike, N. Takegawa, H. Tanimoto,

669   H. Matsueda, S. C. Yoon, and Y. J. Kim, Anthropogenic aerosols observed in Asian

670   continental outflow at Jeju Island, Korea, in spring 2005, J. Geophys. Res., 114,

671   D03301, doi:10.1029/2008JD010306, 2009.

672   Samset, B. H., et al., Modelled black carbon radiative forcing and atmospheric lifetime in

673   AeroCom Phase II constrained by aircraft observations, Atmos. Phys. Chem., 14,

674   12465-12477, 2014.

675 Schwarz, J. P., J. R. Spackman, R. S. Gao, L. A. Watts, P. Stier, M. Schulz, S. M. Davis,

676   S. C. Wofsy, and D. W. Fahey, Global‑scale black carbon profiles observed in the

677   remote atmosphere and compared to models, Geophys. Res. Lett., 37, L18812,

678   doi:10.1029/2010GL044372, 2010.

679 Seinfeld, J.H., and Pandis, S. N., Atmospheric Chemistry and Physics, 2nd ed., John

680   Wiley &Sons, New York, 2006.

681 Shiraiwa M., Y. Kondo, N. Moteki, N. Takegawa, L. K. Sahu, A. Takami, S. Hatakeyama,

682   S. Yonemura, D. R. Blake, Radiative impact of mixing state of black carbon aerosol

683   in Asian outflow, J. Geophys. Res. 113, D24210, doi:10.1029/2008JD010546, 2008.

684 Subramanian, R., G. L. Kok, D. Baumgardner, A. Clarke, Y. Shinozuka, T. L. Campos,

685   C. G. Heizer, B. B. Stephens, B. de Foy, P. B. Voss, and R. A. Zaveri, Black carbon

686   over Mexico: the effect of atmospheric transport on mixing state, mass absorption

687   cross-section, and BC/CO ratios, Atmos. Chem. Phys., 10, 219-237, 2010.

688 Takami A., T. Miyoshi, A. Shimono , N. Kaneyasu , S. Kato, Y. Kajii, S. Hatakeyama,

689   Transport of anthropogenic aerosols from Asia and subsequent chemical

690   transformation. J. Geophys. Res., 112 (D22S31), doi:10.1029/2006JD008120, 2007.

691 Takami, A., et al., Structural analysis of aerosol particles by microscopic observation

692   using a time-of-flight secondary ion mass spectrometer, J. Geophys. Res. Atmos., 118,

693   6726-6737, doi:10.10002/jgrd.50477, 2013.

694 Yoshino, A., A. Takami, K. Sato, A. Shimizu, N. Kaneyasu, S. Hatakeyama, K. Hara, and

695   M. Hayashi, Influence of trans-boundary air pollution on the urban atmosphere in

696   Fukuoka, Japan, Atmosphere, 7, 51, doi:10.3990/atmos7040051, 2016.

697
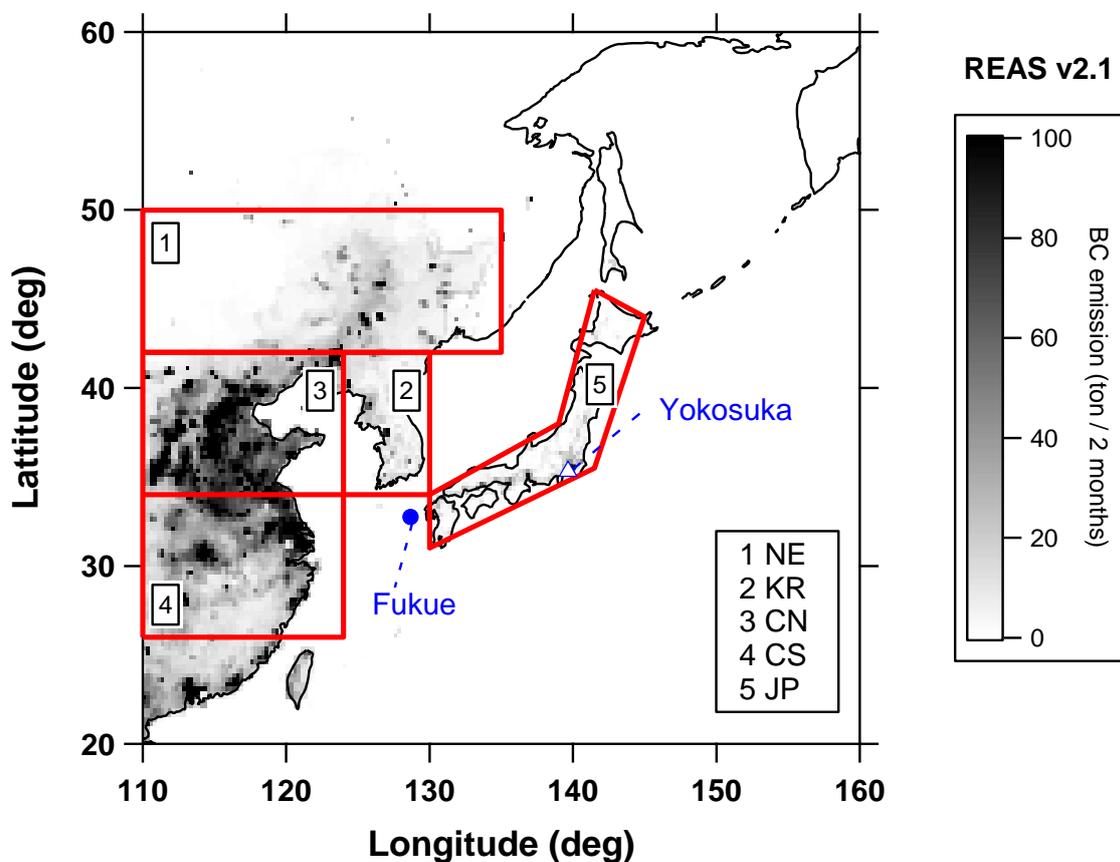
 Figures

699

700

701 **Figure 1.** Map of the investigated region with two observation sites (Yokosuka, open

702 triangle; Fukue Island, closed circle) and five defined areas (1 Northeast China; 2 Korea;

703 3 Central North China; 4 Central South China; 5 Japan). The bimonthly mean BC

704 emission rate (March-April) in 2008 is overlaid on the map (REAS ver. 2.1, Kurokawa et

705 al., 2013).

706
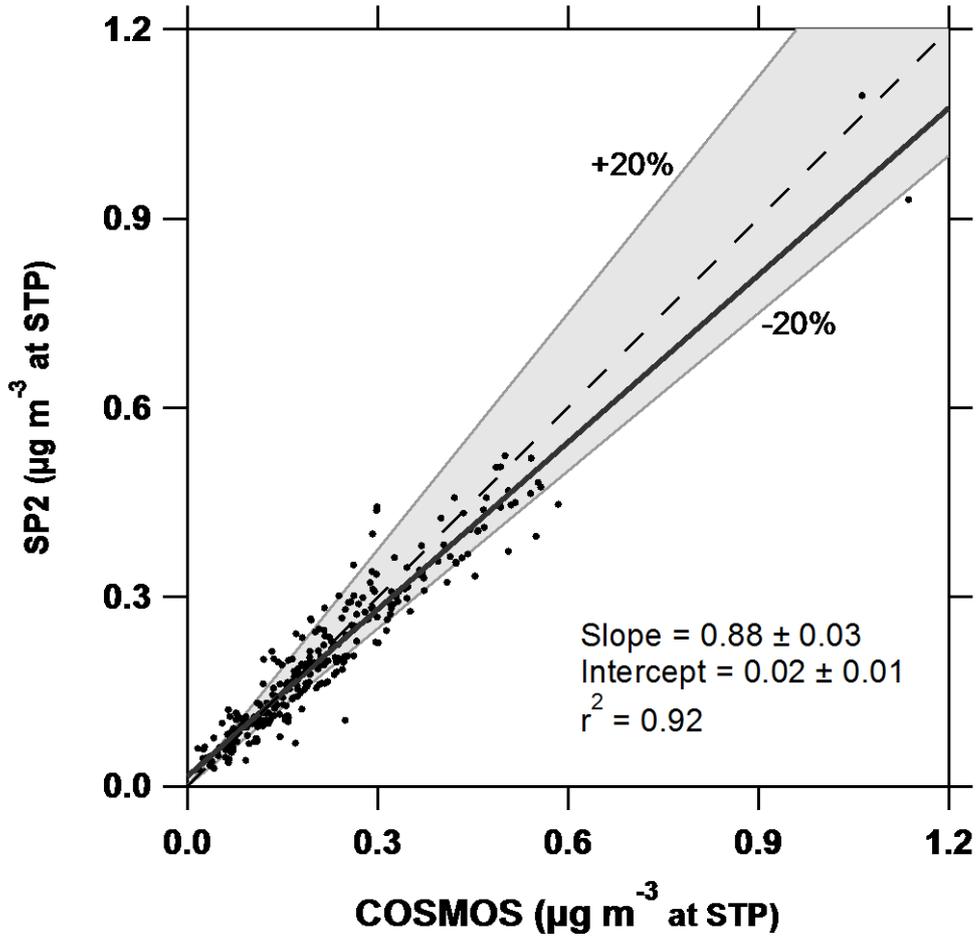
707

708

709 **Figure 2.** Correlation plot of SP2-rBC and COSMOS-EBC mass concentrations (at

710 standard temperature and pressure). The shaded region corresponds to within ±20%.

711

(a) Mean SLP and Mean Wind Velocity (850 hPa)
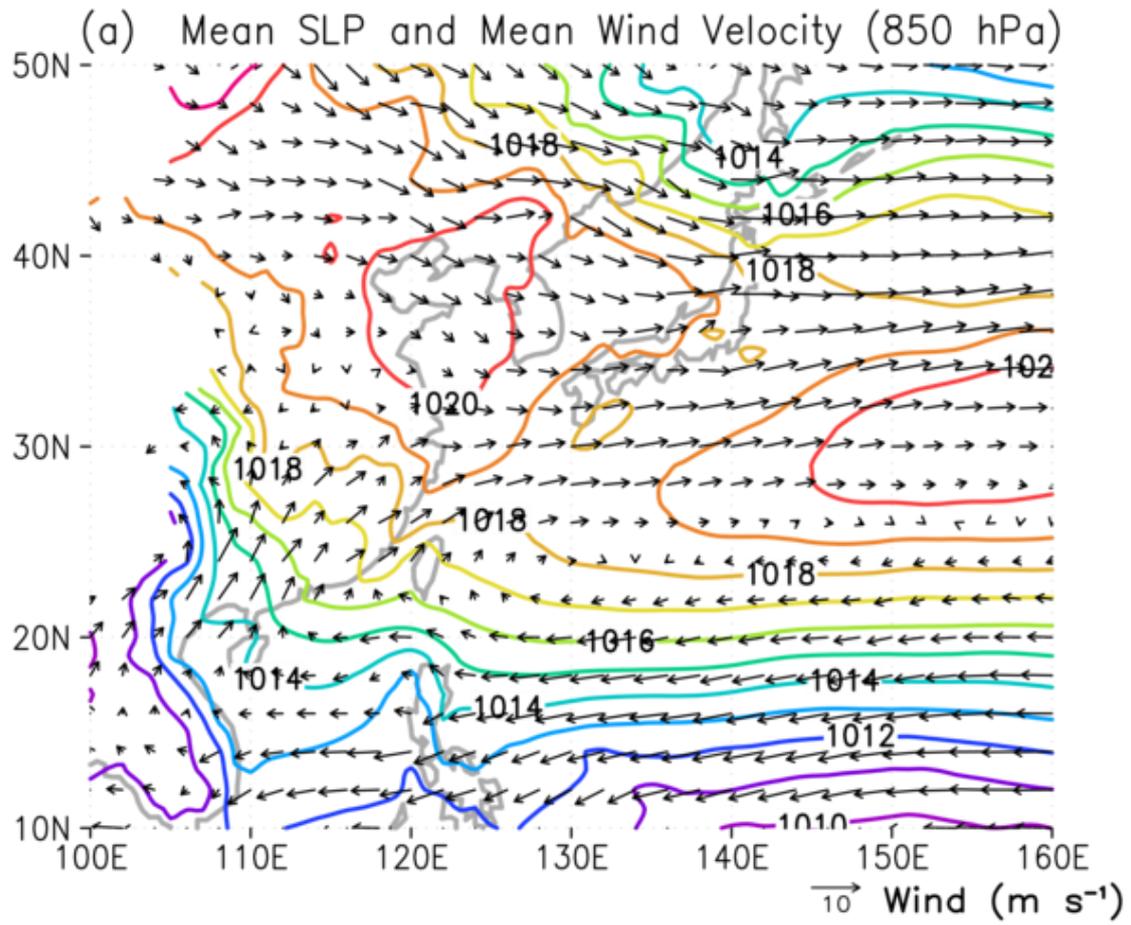
712
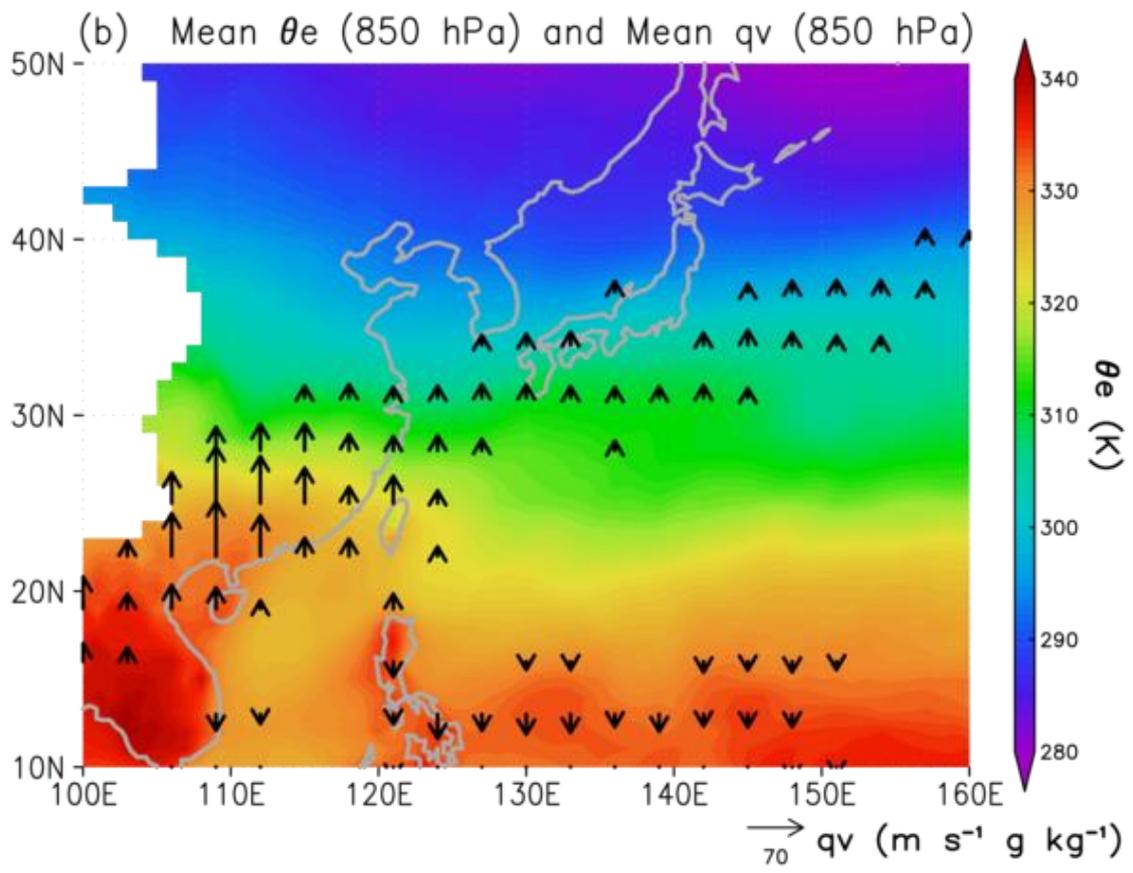
713
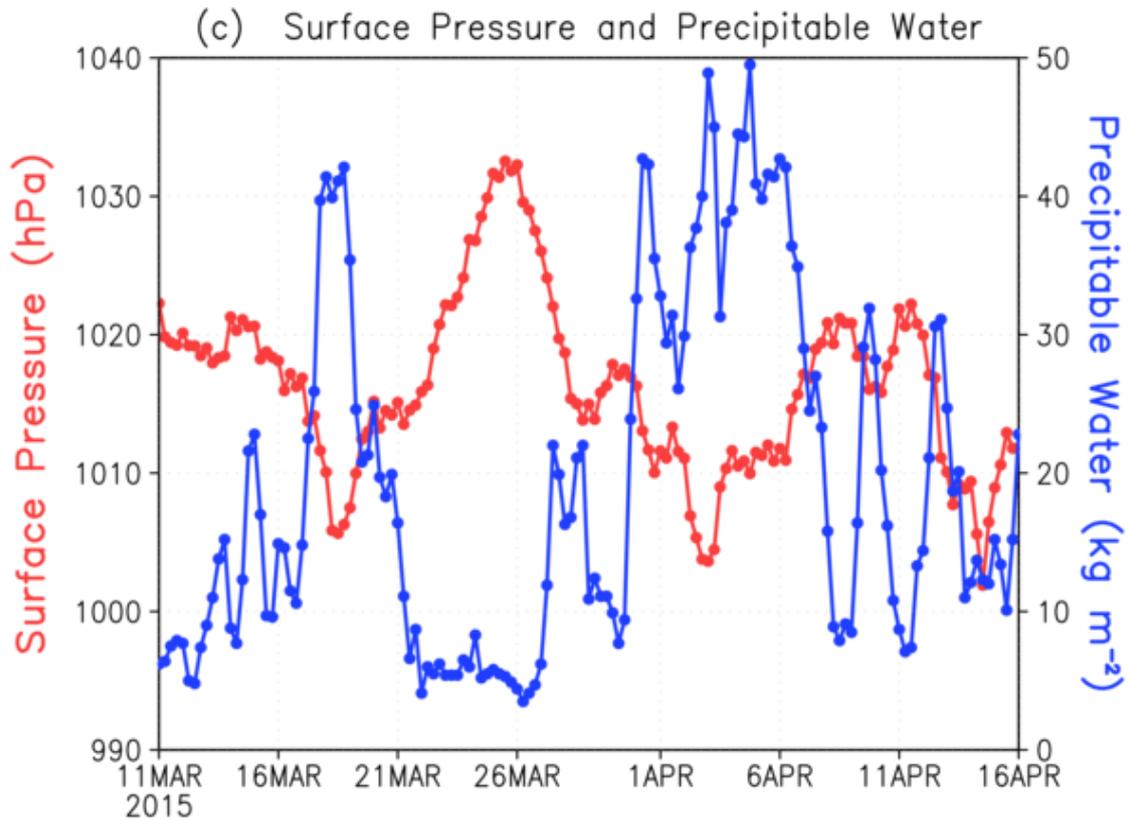
714

715

716 **Figure 3.** Meteorological fields in East Asia during the observation period (March 11-

717 April 14, 2015) based on NCEP FNL data. (a) Mean SLP (hPa, contours) and mean

718 horizontal wind velocity at the 850-hPa level (m s^{-1}). Regions without data correspond

719 to those of high-altitude mountains. (b) Mean θe (K) and total meridional moisture

720 transport (qv values) at the 850-hPa level (m s^{-1} g kg^{-1}). Only qv vectors with

721 magnitudes greater than 10 m s^{-1} g kg^{-1} were plotted. (c) Temporal variations in the

722 surface pressure (hPa, red line and markers with left axis) and precipitable water (kg m^{-2},

723 blue line and markers with right axis) at the Fukue observation site (32.75°N, 128.68°E).

724
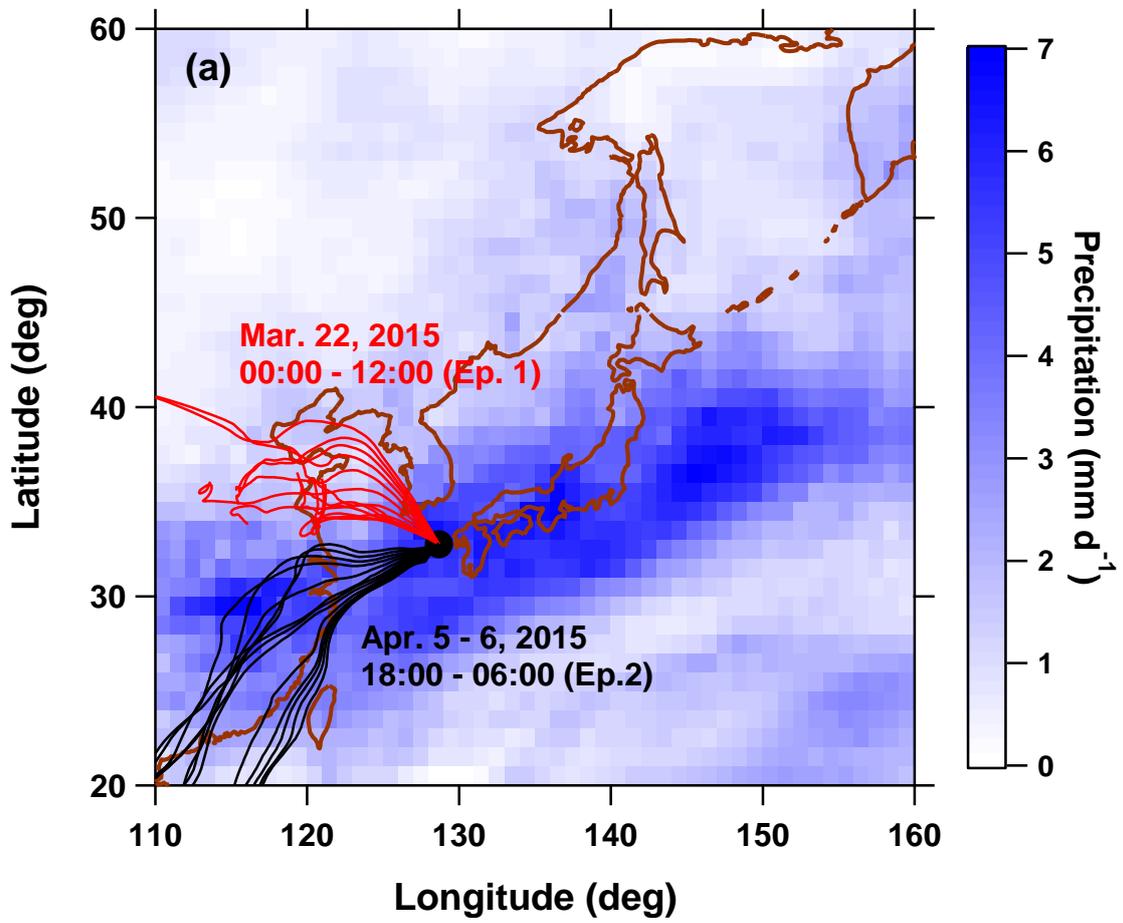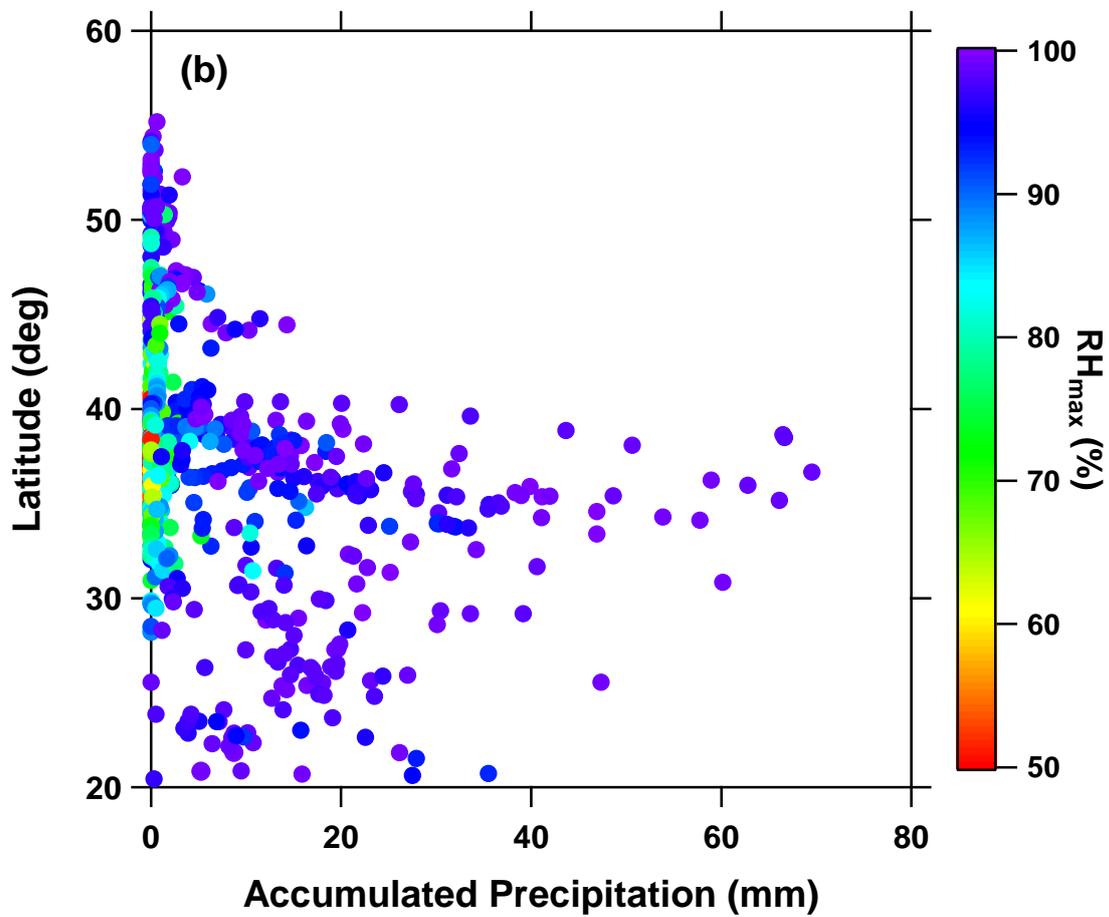
726

727

728 **Figure 4.** (a) Mean precipitation derived from GPCP during the observation period

729 (March 11-April 14, 2015). Three-day backward trajectories for selected periods are

730 overlaid (red lines, 00:00-12:00LT March 22, 2015 (Ep.1); black lines, 08:00LT April 5-

731 06:00LT April 6, 2015 (Ep.2)). (b) The relationship between APT and Lat_{ORIG} (see text

732 for details) colored by the maximum RH along the backward trajectories.

733
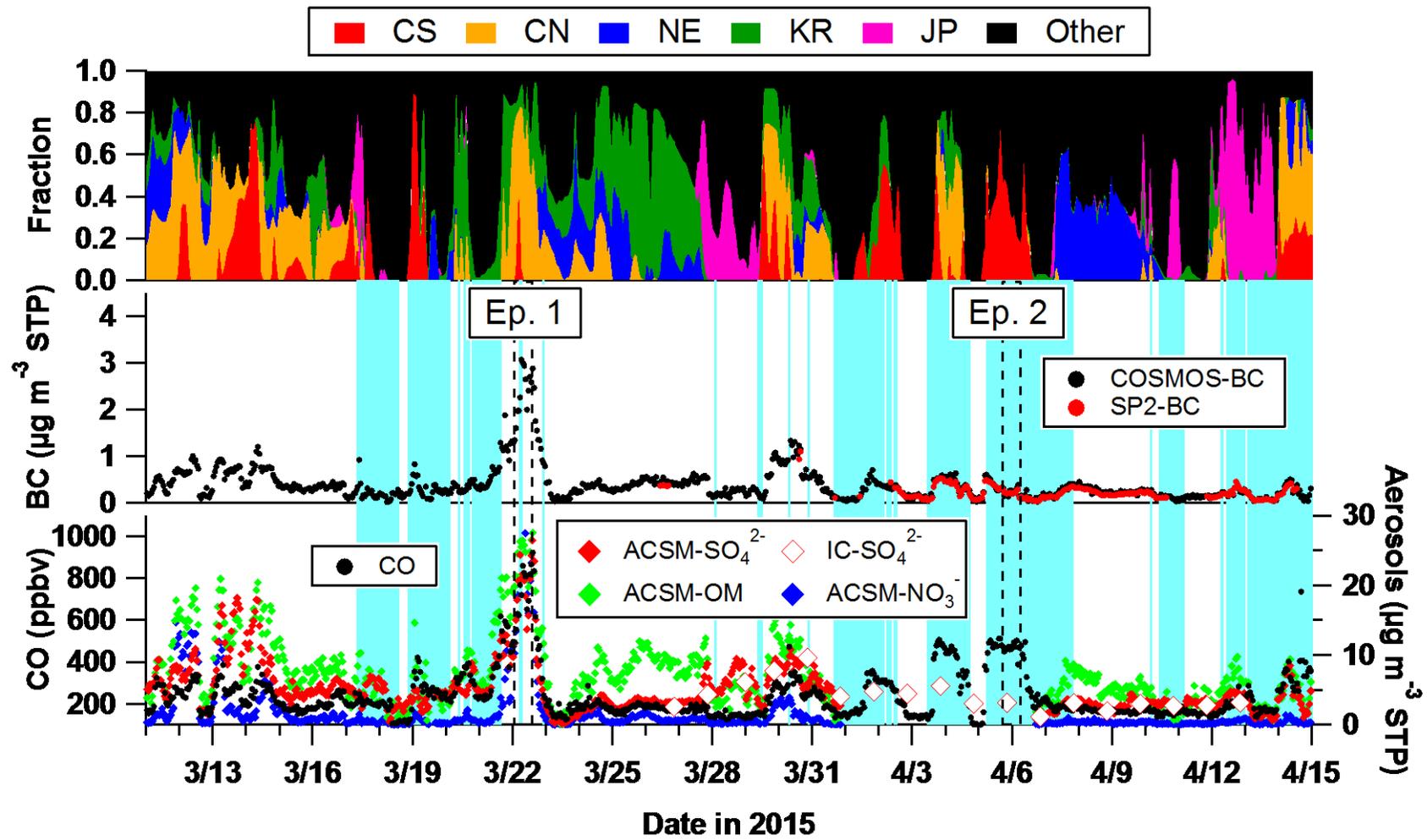
734
735

736   **Figure 5.** Temporal variations in air mass origin and concentration of trace species.   (Top panel) Fractional residence time of air masses

737   passed over selected area (Red, Central South China; Orange, Central North China; Blue, Northeast China; Green, Korea; Pink, Japan;

738   Black, other regions such as Ocean).   (Middle panel) mass concentrations of BC measured using the COSMOS (black markers) and SP2

739   (red markers).   (Bottom panel) concentrations of CO (black markers), SO_4^{2-} (red closed and open makers for ACSM and IC, respectively),

740   ACSM-NO_3^- (blue makers), and ACSM-OM (light green markers).   The periods with the APT > 3 mm are highlighted in light blue in the

741   middle and bottom panels.   The periods denoted as Ep.1 and Ep.2 (see the text for details) were enclosed by dashed lines.
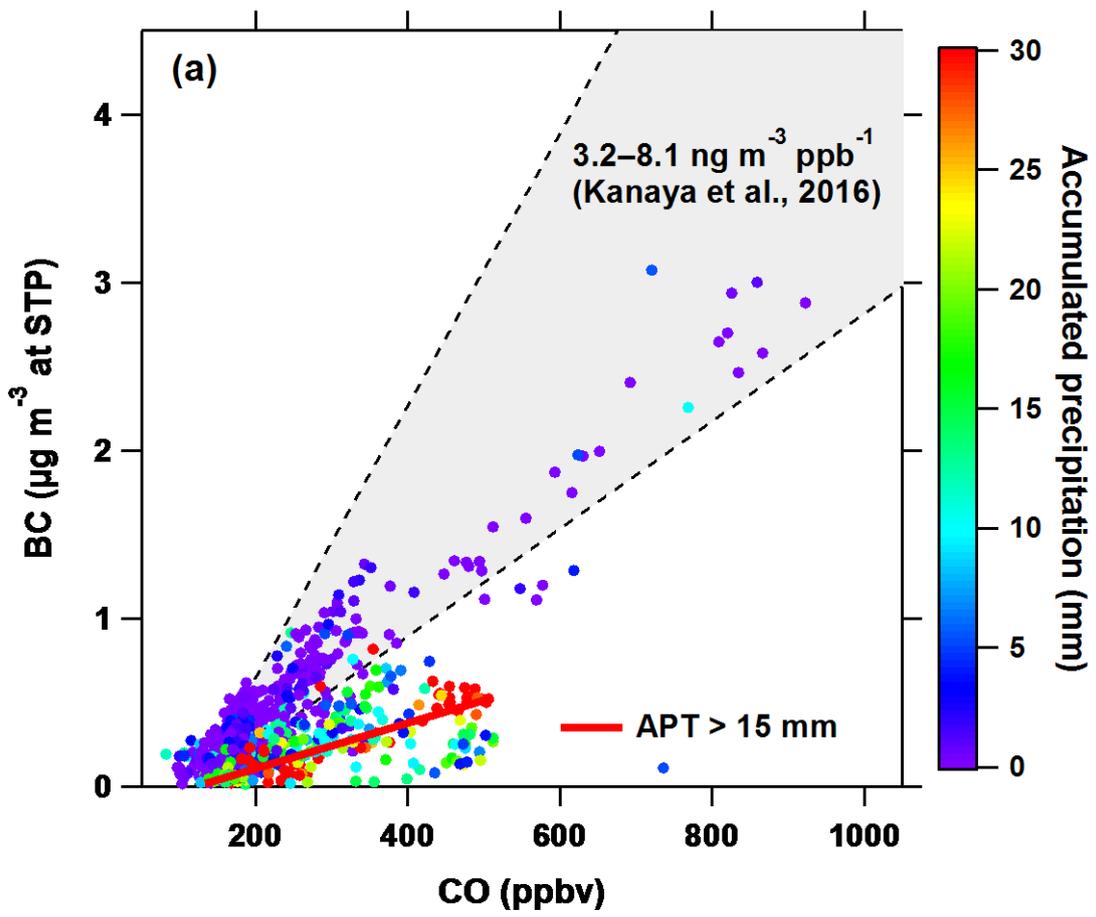
742
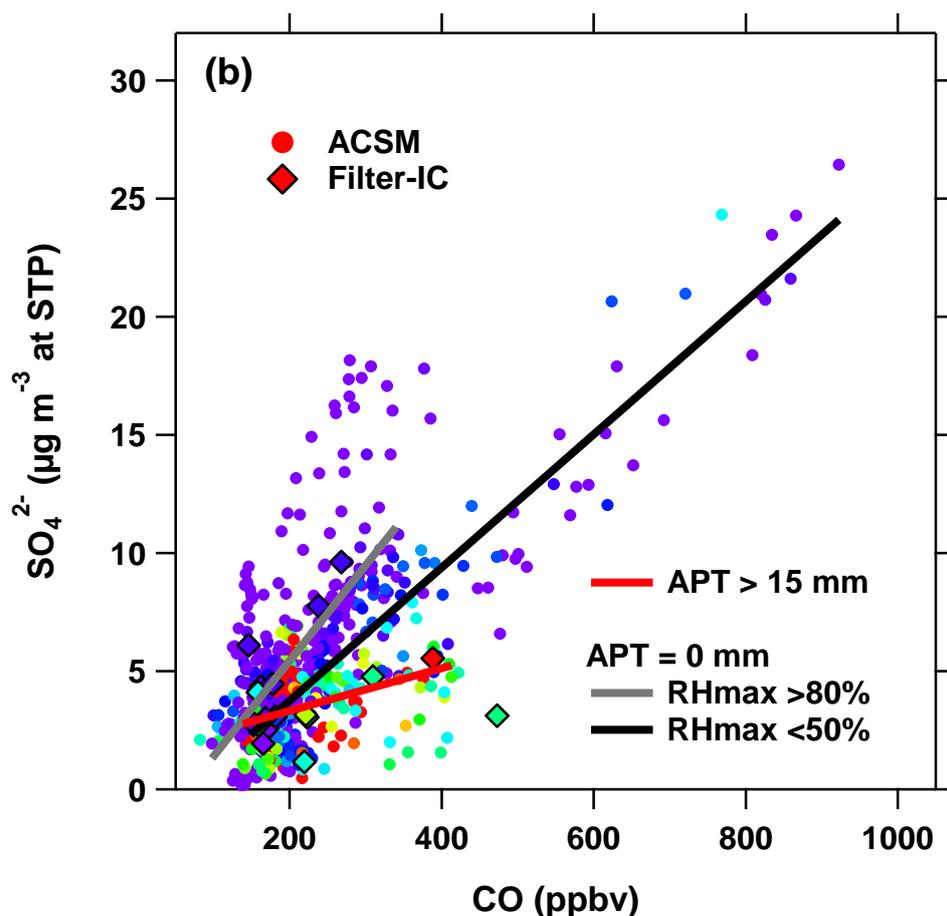
743

744

745 **Figure 6.** Correlation between aerosol mass concentrations and CO mixing ratio colored
746 according to the APT. (a) BC measured by COSMOS and (b) SO_4^{2-} measured by ACSM
747 and IC (circles and diamond markers, respectively). The bold lines are the linear fitting
748 to the BC/CO and ACSM-SO_4^{2-}/CO correlations for the selected data points, i.e., those
749 with the APT >15 mm for BC and SO_4^{2-} (red lines), those with the APT of zero and the
750 RH_{max} <50% for SO_4^{2-} (black line), and those with the APT of zero and the RH_{max} >80%
751 (shaded line).

752
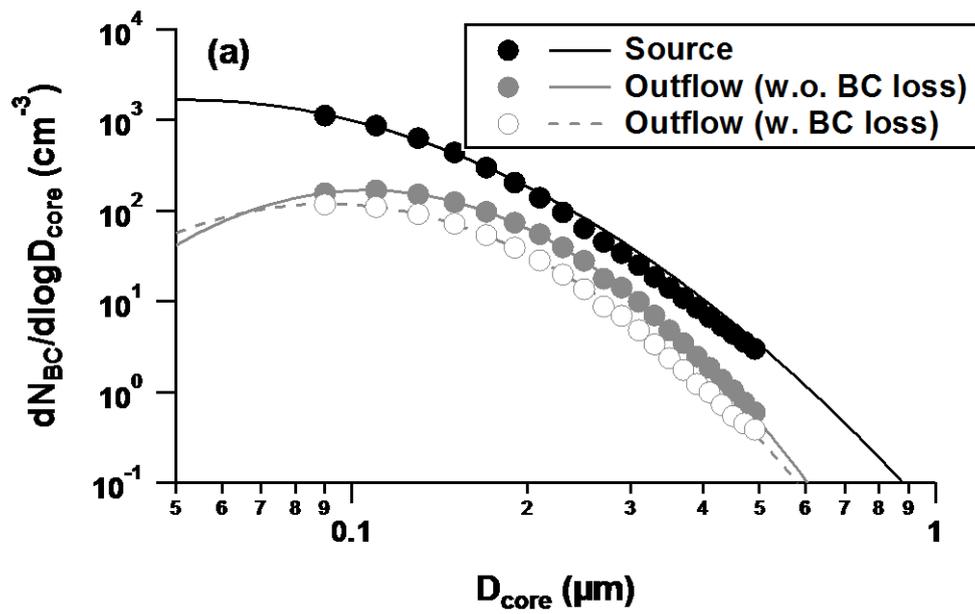
753
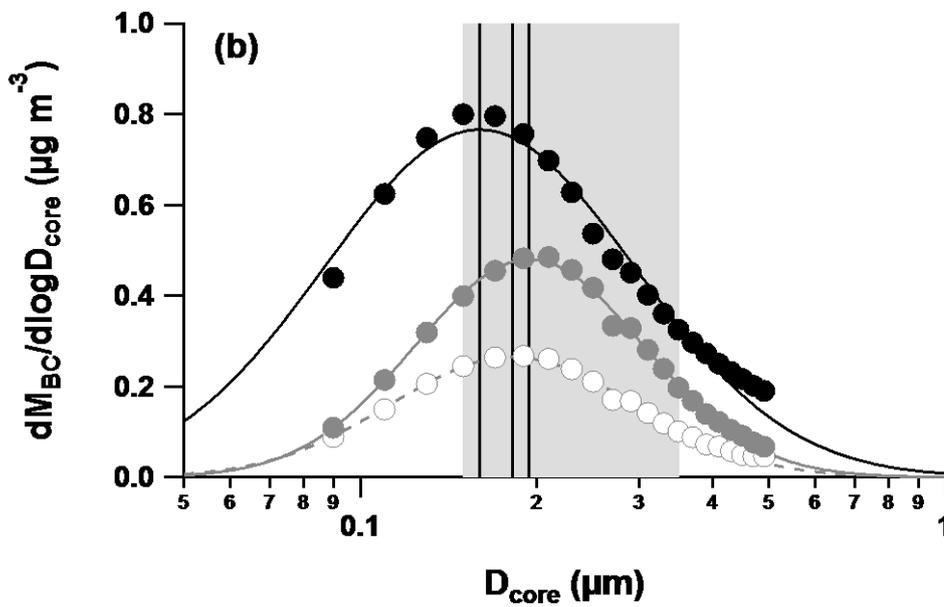
754
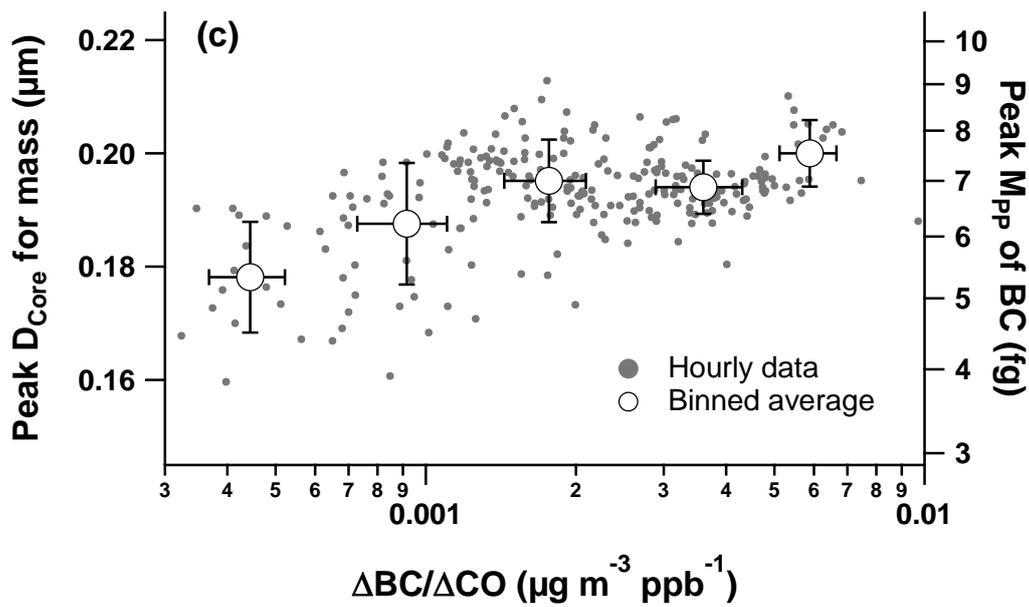
755

756

757 **Figure 7.** The (a) number and (b) mass size distributions of BC measured at Yokosuka

758 (black markers) and at Fukue Island (gray markers).   (c) The evolution of the peak D_{core}

759 as a function of the degree of removal of BC.   The size distributions at Fukue Island

760 include the data for the outflow air masses with (open markers) and without (closed

761 markers) BC loss.   Lines are the lognormal fitting results.   The shaded band in 7(b)

762 corresponds to the size range analyzed to estimate D_s/D_{core} ratios.   Vertical lines in 7(b)

763 represent the peak diameter of the lognormal fit for each of three mass size distributions.

764 Note that the peak diameter of log-normal fit for the BC number size distributions at

765 Yokosuka was estimated from the peak diameter of its mass size distribution (**Table 2**).
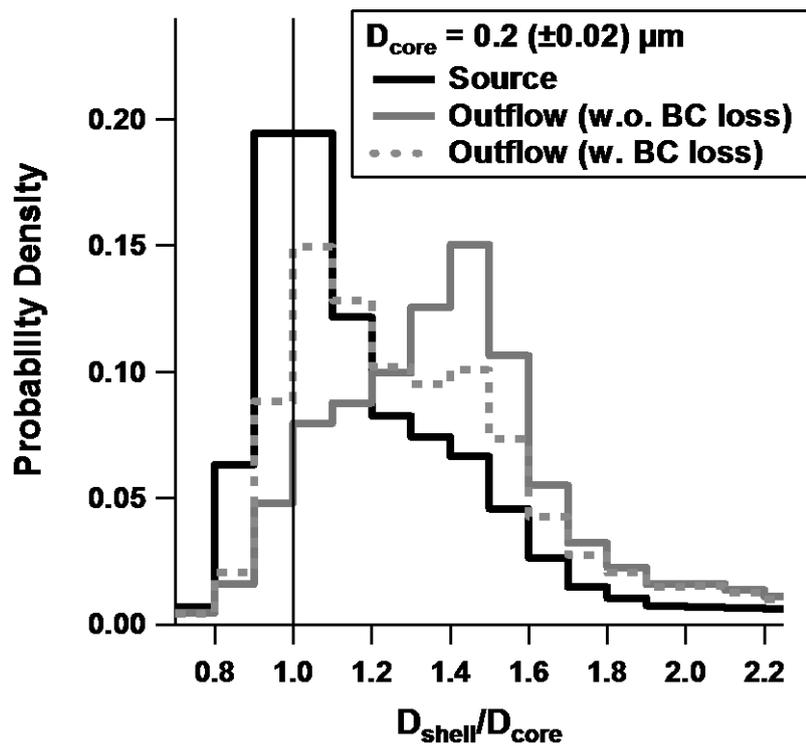
766

767

768   **Figure 8.** Probability density function of the estimated D_s/D_{core} ratios for BC-containing

769   particles with the size 0.2 ($\pm$0.02) μm at Yokosuka (black line) and in the air masses of

770   continental outflow with (gray dashed line) and without (gray solid line) BC loss.

771

772 **Tables**

773 **Table 1. Mean chemical composition of fine aerosols during the observation period**

Componments	Period average	APT			
		0 mm	0 mm RH_{max} <50%	0 mm RH_{max} >80%	>15 mm
Ammonium sulfate	44.9%	41.8%	34.0%	48.9%	50.4%
Ammonium nitrate	11.7%	15.7%	10.7%	8.0%	5.0%
OM	40.9%	40.1%	52.0%	40.4%	42.0%
BC	2.5%	2.4%	3.2%	2.6%	2.5%

774

775

776 **Table 2. Summaries of BC microphysical parameters measured at Yokosuka and Fukue Island**

777

Site	Air mass type	Averaging time* (hrs)	$\Delta BC/\Delta CO$ (ng m^{-3} ppb^{-1})	APT (mm)	Log Normal Fit Parameters Avg. (1σ)		1-hr Median D_S/D_{core} for selected D_{core} Avg. (1σ)			
					MMD (μm)	σ$_g$	0.15 - 0.2	0.2 - 0.25	0.25 - 0.3	0.3 - 0.35 (μm)
Yokosuka	Source	184	-	-	0.160 (0.019)	1.84 (0.08)	1.18 (0.07)	1.15 (0.06)	1.10 (0.04)	1.07 (0.04)
Fukue	Outflow	87	>3	1.2	0.195 (0.005)	1.57 (0.05)	1.37 (0.05)	1.32 (0.03)	1.21 (0.03)	1.17 (0.03)
Fukue	Outflow	51	<1	19.9	0.182 (0.011)	1.62 (0.09)	1.25 (0.05)	1.24 (0.04)	1.16 (0.02)	1.12 (0.03)

778

779 *Time used for calculating averaged statistics of the microphysical properties of BC-containing particles.

780